Miner Deposita (2018) 53:339–352
DOI 10.1007/s00126-017-0743-7

ARTICLE

# Mercury isotope constraints on the source for sediment-hosted lead-zinc deposits in the Changdu area, southwestern China

**Chunxia Xu[1,2] · Runsheng Yin[1,3] · Jiantang Peng[1] · James P. Hurley[3,4] · Ryan F. Lepak[3] · Jianfeng Gao[1] · Xinbin Feng[5] · Ruizhong Hu[1] · Xianwu Bi[1]**

Received: 10 September 2016 / Accepted: 8 May 2017 / Published online: 23 May 2017


**Abstract** The Lanuoma and Cuona sediment-hosted Pb-Zn deposits hosted by Upper Triassic limestone and sandstone, respectively, are located in the Changdu area, SW China. Mercury concentrations and Hg isotopic compositions from sulfide minerals and potential source rocks (e.g., the host sedimentary rocks and the metamorphic basement) were investigated to constrain metal sources and mineralization processes. In both deposits, sulfide minerals have higher mercury (Hg) concentrations (0.35 to 1185 ppm) than the metamorphic basement rocks (0.05 to 0.15 ppm) and sedimentary rocks (0.02 to 0.08 ppm). Large variations of mass-dependent fractionation (3.3‰ in $\delta^{202}$Hg) and mass-independent fractionation (0.3‰ in $\Delta^{199}$Hg) of Hg isotopes were observed. Sulfide minerals have Hg isotope signatures that are similar to the hydrothermal altered rocks around the deposit, and similar to the metamorphic basement, but different from barren sedimentary rocks. The variation of $\Delta^{199}$Hg suggests that Hg in sulfides was mainly derived from the underlying metamorphic basement. Mercury isotopes could be a geochemical tracer in understanding metal sources in hydrothermal ore deposits.

**Keywords** Mercury isotope · Geochemical tracer · Sediment-hosted lead-zinc deposit · Changdu area

Chunxia Xu and Runsheng Yin contributed equally to this work.

Editorial handling: S.-Y. Jiang

**Electronic supplementary material** The online version of this article (doi:10.1007/s00126-017-0743-7) contains supplementary material, which is available to authorized users.

✉ Jiantang Peng
jtpeng@126.com

[1] State Key Laboratory of Ore Deposit Geochemistry, Institute of Geochemistry, Chinese Academy of Sciences, Guiyang 550081, China

[2] University of Chinese Academy of Sciences, Beijing 100039, China

[3] Environmental Chemistry and Technology Program, University of Wisconsin-Madison, Madison, WI 53706, USA

[4] Department at Civil and Environmental Engineering, University of Wisconsin-Madison, Madison, WI 53709, USA

[5] State Key Laboratory of Environmental Geochemistry, Institute of Geochemistry, Chinese Academy of Sciences, Guiyang 550081, China

## Introduction

Sediment-hosted Pb-Zn deposits contain half of the global resources of Zn and Pb (Singer 1995). A fundamental but unanswered question for these deposits is whether the metal-bearing fluids that formed the deposits required specific source rocks enriched in extractable metals (Leach et al. 2005, 2010). Although Pb isotopes have been utilized to trace metal sources for these deposits, information from Pb isotopes indicates that Pb was derived from a variety of crustal sources (e.g., Deloule et al. 1986; Kesler et al. 1994; Krahn and Baumann 1996; Bouhlel et al. 2016). Up to now, few studies have provided direct evidence for specific source rocks for the ore metals in the sediment-hosted Pb-Zn deposits (Leach et al. 2010), which seriously hampers our further understanding of ore genesis for these deposits.

Unlike Pb isotopes, Hg isotopes can undergo both mass-dependent fractionation (MDF, termed as $\delta$ values) and mass-independent fractionation (MIF, termed as $\Delta$ values) during various physical, chemical, and biological processes, which could provide multi-dimensional information on sources and geochemical processes (e.g., Bergquist and Blum 2007; Zheng et al. 2007; Das et al. 2009; Foucher et al. 2009;

Gantner et al. 2009; Estrade et al. 2010; Feng et al. 2010; Yin et al. 2010; Hintelmann and Zheng 2012). Large variations of 10‰ for both $\delta^{202}$Hg and $\Delta^{199}$Hg values were observed in natural samples (Blum et al. 2014). It is interesting that natural samples with significant MIF are mainly found in the Earth's surface (e.g., soil, sediment, peat, etc.) and near surface environment (e.g., coal, black shale). In contrast, magmatic Hg source has been shown $\Delta^{199}$Hg close to zero (Yin et al. 2016). Photochemical reactions are the main processes to generate Hg-MIF in the environment (Blum et al. 2014). Since Hg is a global pollutant, Hg isotopes have often been used by environmental geochemists to trace sources and processes of Hg pollution (e.g., Foucher et al. 2009; Feng et al. 2010; Pribil et al. 2010; Sonke et al. 2010). However, application of Hg isotopes to other fields such as ore deposit geochemistry is still in its infancy. To date, only a few studies have documented Hg isotopes in Hg ore deposits (Hintelmann and Lu 2003; Smith et al. 2005, 2008; Sherman et al. 2009; Yin et al. 2013), and other deposits including Pb-Zn have rarely been studied for their Hg isotope composition (Sonke et al. 2010; Yin et al. 2016; Tang et al. 2017).

Mercury, as a chalcophile element, is usually enriched in sulfide minerals (Rytuba 2003), and sphalerite is the chief host for Hg in Pb-Zn deposits (Schwartz 1997; Grammatikopoulos et al. 2006). Previous studies have reported dramatic Hg-MDF ($\delta^{202}$Hg ~2.6‰) and small but significant Hg-MIF ($\Delta^{199}$Hg ~0.4‰) in sphalerite from numerous Pb-Zn deposits worldwide (Sonke et al. 2010; Yin et al. 2016; Tang et al. 2017). The MIF signature of Hg isotopes has been demonstrated as a useful tracer in distinguishing magmatic from sedimentary Hg sources (Yin et al. 2016). In a recent study by Yin et al. (2016), the isotopic signatures of Hg were characterized for different types of Pb-Zn deposits including sedimentary exhalative deposits (SEDEX), Mississippi Valley-type deposits (MVT), volcanic-hosted massive sulfides deposits (VMS), and intrusion-related deposits (IR). Specifically, SEDEX and MVT deposits have more pronounced MIF (0.42% in $\Delta^{199}$Hg values), and the MIF was linked to Hg from sedimentary sources. VMS and IR deposits showed the absence of significant MIF, which is consistent with magmatic sources. Although previous studies reported Hg isotopic differences for various deposits, the isotopic variation of Hg within a single deposit was rarely studied. Mercury is usually distributed heterogeneously in minerals, and the variation of Hg isotopes in individual deposits is still unclear. Hence, systematic studies of Hg concentration and isotopic composition are necessary for understanding the geochemical processes of Hg in ore deposits.

We carried out an integrated investigation of Hg concentrations and isotopic compositions for different sulfides and rocks in two sediment-hosted Pb-Zn deposits, Lanuoma and Cuona from the Changdu area, SW China. This is the first study to use Hg-MIF to trace metal sources in two individual ore deposits. We aim to investigate whether Hg isotopes can be used to trace metal sources and ascertain ore-forming processes.

## Geological setting

The NW-trending Sanjiang tectono-magmatic belt lies between the Jinshajiang and Bangonghu-Nujiang sutures along the eastern and northern margins of the Tibetan Plateau (Fig. 1a), which is an important Pb-Zn mining region within the Tibetan-Himalayan metallogenic domain (Hou et al. 2007; Hou and Cook 2009). The Changdu area is located in the northern part of the Sanjiang tectono-magmatic belt (Fig. 1a). The oldest rocks outcropped in this area are Precambrian basement rocks of the Jitang Group, which are composed mainly of schist, granulite, and gneiss (Fig. 1b). Other strata exposed in the area include late Paleozoic to Cenozoic sedimentary rocks. Late Paleozoic strata are dominated by shallow marine carbonate and clastic rocks (Peng et al. 2000). Mesozoic strata contain Triassic shallow marine carbonate rocks and sandy mudstones, Jurassic marine-terrestrial to terrestrial clastic rocks, and Cretaceous fluvial sediments (Du et al. 1997). The Tertiary strata mainly consist of clastic rocks and gypsum (Peng et al. 2000).

Large-scale NW-striking thrust nappes formed during the Cenozoic Indo-Asian collision (Hou et al. 2008). The major thrust nappes contain two thrust systems with opposite dips termed as the eastern and western thrust faults (Tang et al. 2006). Igneous rocks are mainly Triassic granitic rocks and Cenozoic granites formed during the extension of thickened crust after the closure of the Paleo-Lancangjiang ocean and the Himalayan collision, respectively (Tao et al. 2011).

## Geology of ore deposits

### *Lanuoma deposit*

The Lanuoma deposit is located approximately 10 km north of Jitang Town and has an estimated resource of 0.47 Mt Pb+Zn and 0.17 Mt Sb according to the geological survey of the Tibet Autonomous Region (Feng 2006). The stratigraphic sequence at Lanuoma contains four Upper Triassic formations including Jiapila, Bolila, Adula and Duogaila, and Quaternary alluvium (Fig. 2). The lowermost unit, Jiapila Formation, is mainly comprised of fluvial lithic, feldspathic quartz sandstone. The overlying Bolila Formation, as ore-hosting strata, consists of shallow marine conglomeratic and fine-grained limestone, which is overlain by the Adula Formation. The Adula Formation is dominated by alternating continental-marine silty shale with intercalation of feldspathic quartz sandstone, unconformably overlain by the delta lithic sandstone, silty mud shale of the Duogaila Formation. No igneous rocks are exposed in the mining area.

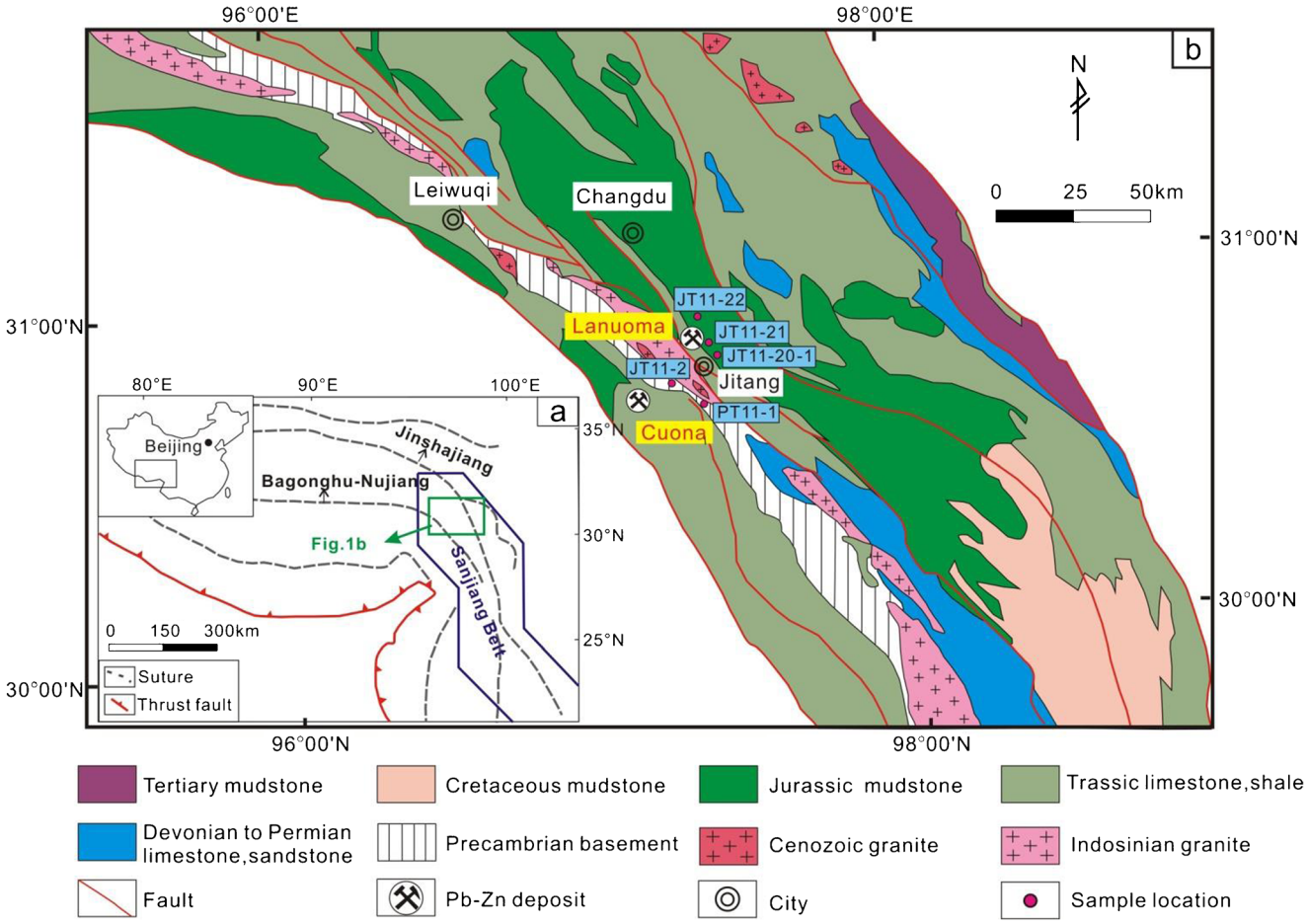


**Fig. 1** Geologic map of the Changdu area showing the Lanuoma and Cuona deposits localities and sample locations (**a**, modified after Spurlin et al. 2005; **b**, after Tao et al. 2011)

Two fault systems are dominant in the area, striking north and east, respectively (Fig. 2). The north trending thrust faults ($F_1$, $F_2$) provide space for the emplacement of the primary ore bodies, while the east trending strike-slip fault ($F_3$) controls the distribution of the secondary oxide ore bodies (Tao et al. 2011). Two ore bodies are delineated in the mining area, namely No. I and No. II, with an average grade of 1.90% Pb, 3.04% Zn, and 1.86% Pb, 1.08% Zn, respectively.

The Lanuoma deposit is an epigenetic and stratabound deposit. Ore bodies are hosted in fracture zones with banded and stratiform shape. The mineralization mainly occurs as open-space fillings, with subordinate replacement, and displays vein (Fig. 3a), breccia (Fig. 3b), massive (Fig. 3c), and disseminated (Fig. 3d) styles. Ore minerals are usually coarse-grained sphalerite, robinsonite ($Pb_4Sb_6S_{13}$), with minor galena, pyrite, orpiment, and trace realgar. Sphalerite ranges in color from yellow to brown with subhedral crystals from sub-millimeter to several millimeters in size. Robinsonite is anhedral and generally 2 to 3 mm in diameter. Sphalerite is usually replaced by robinsonite as relict textures (Fig. 3e, f), indicating that sphalerite formed prior to robinsonite. Gangue minerals are mainly calcite with minor quartz, barite, and dolomite.

*Cuona deposit*

The Cuona deposit is located in Basu County, Tibet, and has an estimated resource of 0.17 Mt Pb, 0.09 Mt Zn, and 552 t Ag according to the geological survey of the Tibet Autonomous Region (Feng 2006). The stratigraphic sequence at Cuona mainly includes the Upper Triassic Adula Formation, Cretaceous Basu Formation, and Quaternary alluvium and diluvium (Fig. 4). The Adula Formation consists of feldspathic quartz sandstone, siltstone, shale, slate, and hornfels, which is unconformably overlain by the Basu Formation, the latter is mainly comprised of sandy conglomerate and pebbly sandstone. Three NW-SE trending thrust faults ($F_1$, $F_2$, $F_3$) occur in the mining area (Fig. 4). The $F_1$ fault serves as main ore fluid conduit, and the $F_2$ and $F_3$ faults host the ore. Igneous rocks exposed in the mining area include late Yanshanian granite and several late Himalayan granite porphyry dykes.

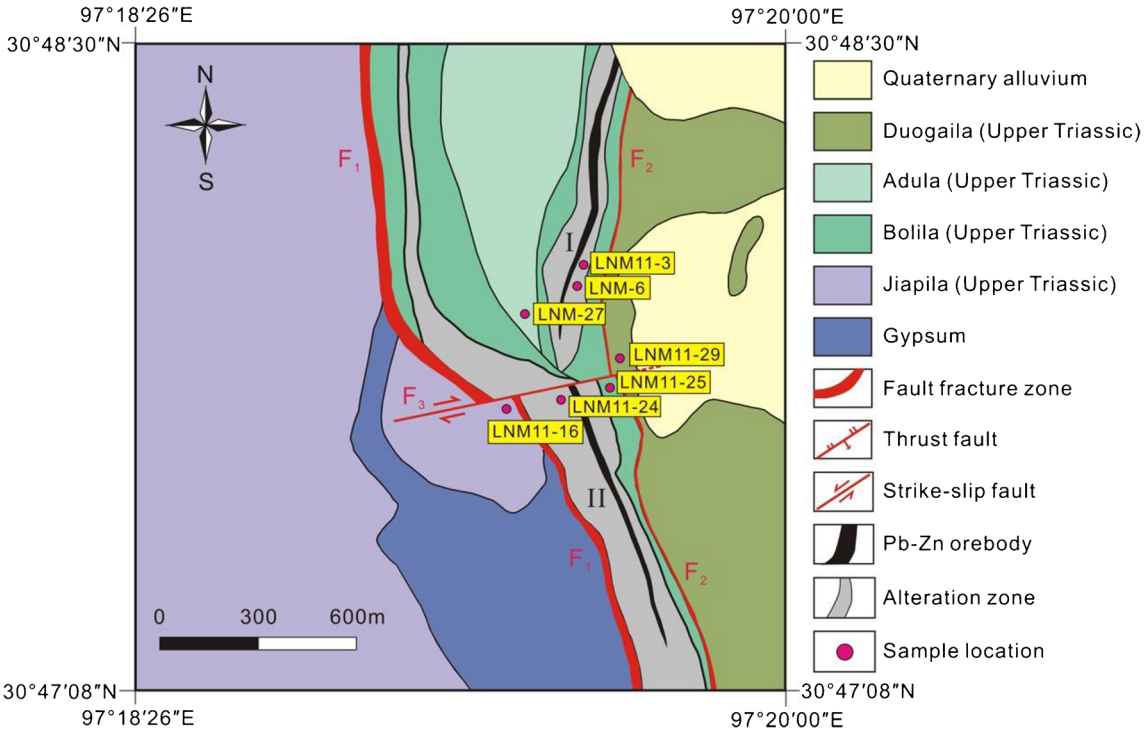


**Fig. 2** Geologic map of the Lanuoma deposit and sample locations (modified from Feng 2006)

Three ore bodies have been delineated including No. I ore body grading 8.6% Pb, 6.7% Zn, and 12 g/t Ag; No. II averaging 3.3% Pb and 1.7% Zn; and No. III with Pb ranging from 0.6 to 5.0%, Zn from 0.5 to 10.5%, and Ag from 20 to 180 g/t. The Cuona deposit is also an epigenetic and stratabound deposit. Ore bodies usually occur as stratiform, composite, and banded

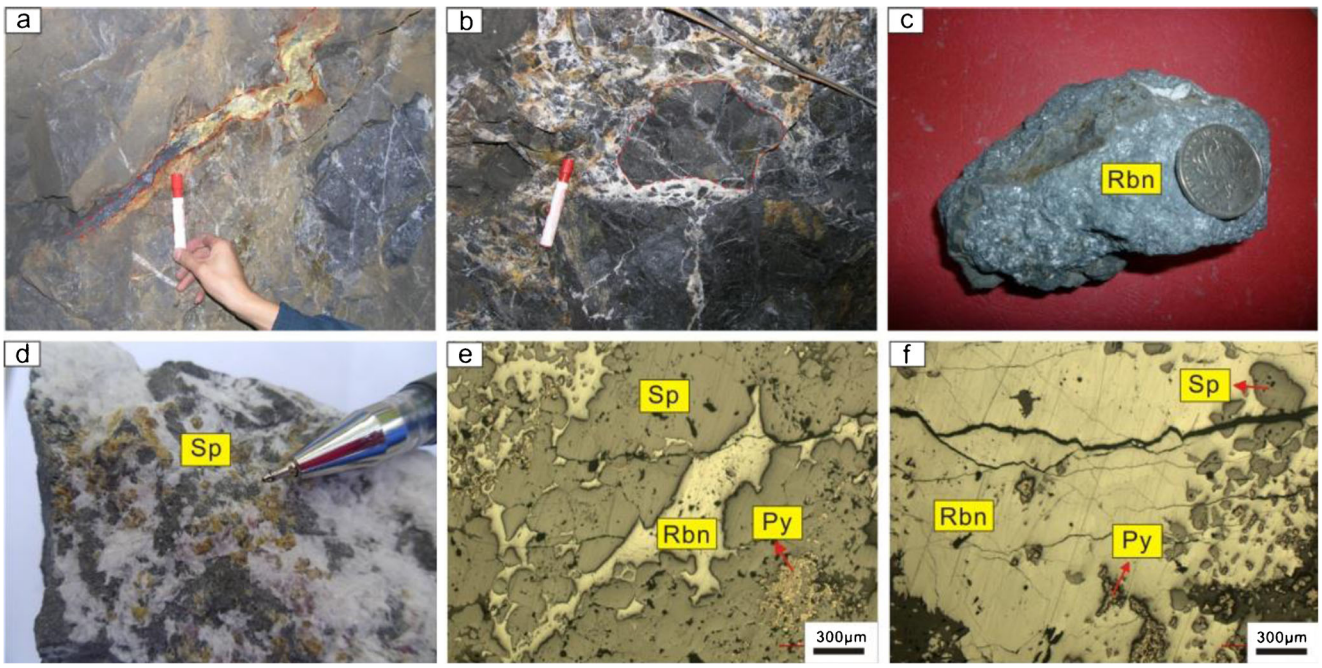


**Fig. 3** Macroscopic photographs and reflected light photomicrographs of ore samples from the Lanuoma deposit. **a** Vein type ore (underground). **b** Brecciated ore (underground). **c** Massive robinsonite (hand specimen). **d** Disseminated sphalerite in calcite. **e** Robinsonite replacing sphalerite along its fractures (reflected light). **f** Sphalerite and pyrite replaced by robinsonite as metasomatic texture (reflected light). *Py* pyrite, *Rbn* robinsonite, *Sp* sphalerite

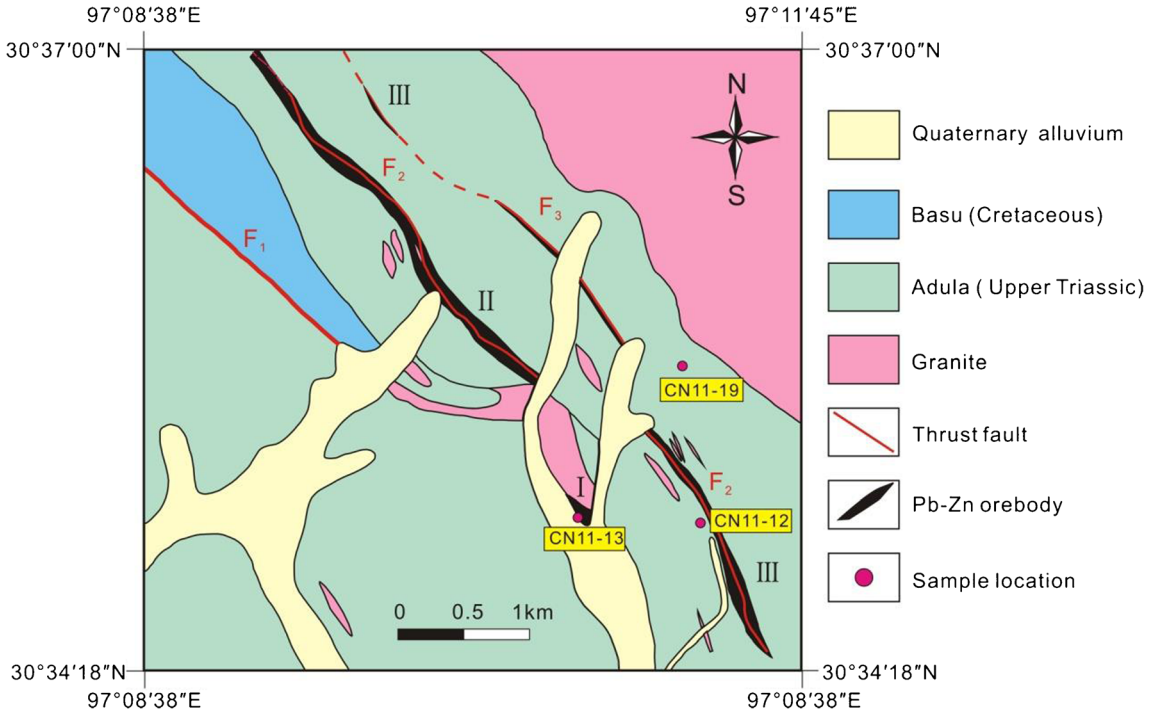


**Fig. 4** Geologic map of the Cuona deposit and sample locations (modified from Feng 2006)

veins and are concordant with the $F_2$ fault. Mineralization occurs as open-space fillings and displays massive (Fig. 5a), breccias, vein (Fig. 5b), and disseminated styles (Fig. 5c). Ore minerals include coarse-grained galena and sphalerite, and fine-grained pyrite with minor chalcopyrite and argentite. Sphalerite from the Cuona deposit ranges in color from brown

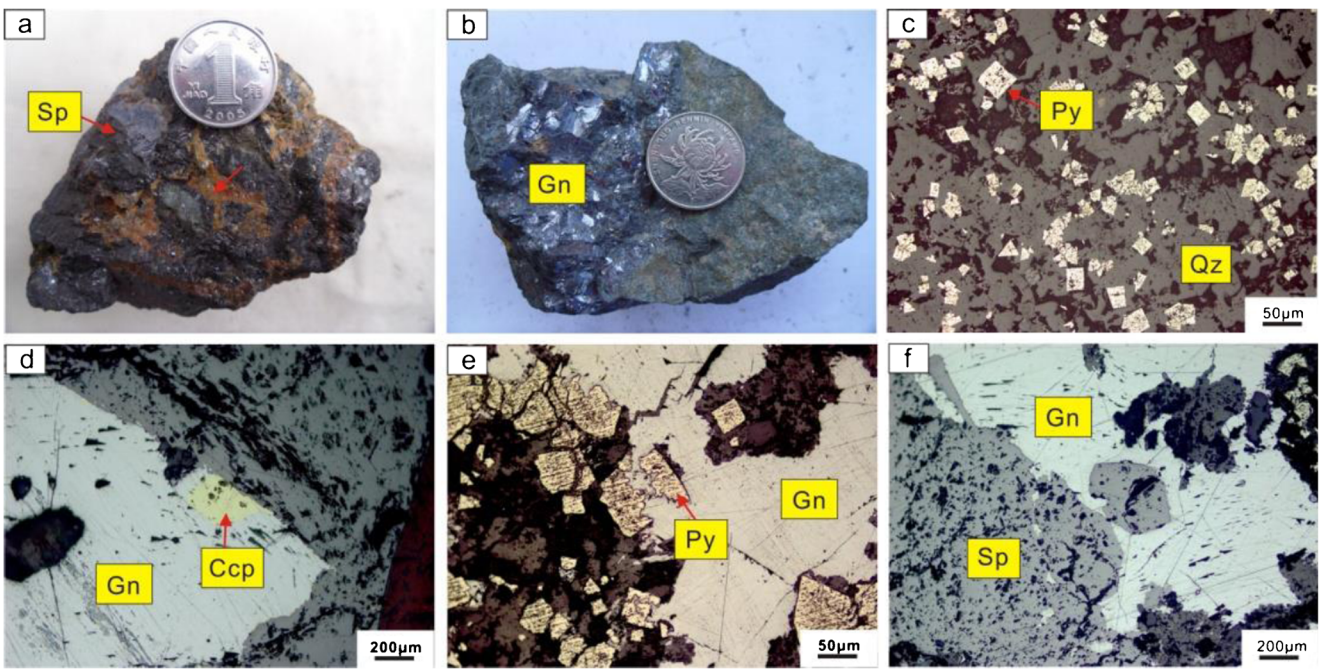


**Fig. 5** Macroscopic photographs and reflected light photomicrographs of ore samples from the Cuona deposit. **a** Stockwork ore (hand specimen). **b** Vein of coarse-grained galena filling in quartz sandstone (hand specimen). **c** Disseminated fine-grained pyrite in quartz sandstone (reflected light). **d** Coexisting of galena and sphalerite, chalcopyrite replacing galena (reflected light). **e** Pyrite replaced by galena (reflected light). **f** Galena replacing sphalerite (reflected light). *Ccp* chalcopyrite, *Gn* galena, *Py* pyrite, *Sp* sphalerite

to tan. Sphalerite and galena are usually coexisting and have subhedral to euhedral crystals with size from 1 mm to several millimeters in diameter. Gangue minerals contain quartz with minor barite, sericite, and kaolinite. Although replacement textures among sulfides are common (Fig. 5d–f), it is very difficult to distinguish the mineral-paragenetic sequence.

Those sediment-hosted lead-zinc deposits in the Sanjiang region were considered to be formed during the Cenozoic (Hou et al. 2008). Unfortunately, due to lack of suitable minerals for radiometric dating, the mineralization ages of both deposits in this study are unavailable.

## Sampling and analytical methods

In the Lanuoma mining district, ten ore samples were collected from the underground exposures in different levels. Seven wall rock samples, including four altered rocks (LNM11-16, LNM11-3, LNM-6, LNM11-24) and three barren rocks (LNM11-25, LNM11-27, LNM11-29), were collected from the outcrop in mining district. Sample location and description are documented in Table A1 (Electronic supplementary material). Because the Cuona deposit had ceased to be exploited, eight ore samples in this study were collected from ore dump in the gallery and three wall rock samples, including two altered rocks (CN11-12, CN11-13) and one barren rock (CN11-19), were collected from the outcrop in the mining district. Sample location of wall rocks is marked in Fig. 4, and sample descriptions of ore and wall rocks are briefly documented in Table A2 (Electronic supplementary material). Two metamorphic rocks and three Jurassic rocks were collected from the distal regional outcrop near the Jitang town. Sample location of these rocks is shown in Fig. 1b, and sample description is shown in Table A3 (Electronic supplementary material).

The weight of each sample ranges from 2 to 5 kg. In the laboratory, ore samples were crushed, and sulfide minerals were separated by hand-picking under a binocular microscope, and about 2 g of each sulfide separate was picked and manually crushed into 150 mesh in an agate mortar prior to analysis. For rock samples, about 1 kg of each sample was crushed and sieved to 150 mesh. Total Hg (THg) concentrations were measured by cold vapor atomic absorption spectrometry (CVAAS) in the Institute of Geochemistry, Chinese Academy of Sciences (CAS), following the method described by Li et al. (2005). The recoveries of THg for standard reference materials GBW0715 (high grade lead-zinc ore, $n$ = 3) and GBW07168 (Zn concentrates, $n$ = 3) are 97 to 102%. The relative variability of sample duplicates is <8%.

Approximately 0.1 to 0.2 g of each sample was digested in a plastic centrifuge tube (Corning® 50-mL PP centrifuge tubes) using 5-mL aqua regia ($HCl/HNO_3$ = 3:1, $v/v$). The tubes were then heated in a water bath (95 °C) for 12 h. Standard reference material NIST-2711 (Montana soil II) was prepared in the same way. An aliquot was removed from each digest and diluted to 1 ng $mL^{-1}$ of Hg prior to Hg isotope measurement by a Thermo Scientific Neptune Plus multi-collector inductively coupled plasma mass spectrometry (MC-ICP-MS) at the Wisconsin State Lab of Hygiene, University of Wisconsin-Madison. Mercury concentrations were monitored by $^{202}Hg$ signals, and the $^{202}Hg$ intensities ranged from 1.0 to 1.2 V for 1 ng $mL^{-1}$ Hg, and $^{202}Hg$ signals for blanks were about $1.0 \times 10^{-3}$ V. The diluted solutions were prepared to have acid concentration of 10 to 20%, and Hg concentrations and acid matrices of the NIST-3133 standard solutions were matched to the bracketed samples. Details of methods and instrumental conditions were previously reported by Yin et al. (2016). THg concentrations in digest solutions were monitored by $^{201}Hg$ intensities during Hg isotope analysis, which were with ±10% (1SD) of that measured by CVAAS. Hg-MDF is reported in delta notation in per mil (‰), referenced to the NIST-3133 Hg standard, and analyzed before and after each sample following the convention recommended by Blum and Bergquist (2007),

$$\delta^{xxx}\mathrm{Hg}(‰) = \left[\left({}^{xxx}\mathrm{Hg}/{}^{198}\mathrm{Hg}\right)_{\mathrm{Sample}} / \left({}^{xxx}\mathrm{Hg}/{}^{198}\mathrm{Hg}\right)_{\mathrm{SRM3133}} - 1\right] \times 1000 \quad (1)$$

where xxx is the mass of each Hg isotope from 199 to 202 amu. Hg-MIF is reported using "capital delta" notation ($\Delta^{xxx}Hg$), which represents the deviation from mass dependency in units of per mil (‰) (Blum and Bergquist 2007), where:

$$\Delta^{199}\mathrm{Hg} = \delta^{199}\mathrm{Hg} - 0.2520 \times \delta^{202}\mathrm{Hg} \quad (2)$$

$$\Delta^{200}\mathrm{Hg} = \delta^{199}\mathrm{Hg} - 0.5024 \times \delta^{202}\mathrm{Hg} \quad (3)$$

$$\Delta^{201}\mathrm{Hg} = \delta^{201}\mathrm{Hg} - 0.7520 \times \delta^{202}\mathrm{Hg} \quad (4)$$

Replicate measurements of the UM-Almadén secondary standard solution were also measured. Data uncertainty reported in this study reflects the larger value of either the external precision of replication of the UM-Almadén solution or the sample digests. The overall mean and uncertainty of UM-Almadén ($\delta^{202}Hg$, −0.52 ± 0.08‰; $\Delta^{199}Hg$, −0.03 ± 0.06‰; $\Delta^{201}Hg$, −0.01 ± 0.06‰, 2σ, $n$ = 11) and NIST-2711 ($\delta^{202}Hg$, −0.20 ± 0.06‰; $\Delta^{199}Hg$, −0.19 ± 0.06‰; $\Delta^{201}Hg$, −0.17 ± 0.03‰, 2σ, $n$ = 3) are comparable with previous studies (Blum and Bergquist 2007; Yin et al. 2014).

# Results

## Hg concentrations

THg concentrations of regional metamorphic basement, Upper Triassic, and Jurassic rocks are shown in Table 1.

**Table 1** Hg concentrations and Hg isotopic compositions of potential source rocks from Changdu area

| Sample no. | Description | THg (ppm) | Pb (ppm) | Zn (ppm) | $\delta^{202}$Hg (‰) | 2SD (‰) | $\Delta^{199}$Hg (‰) | 2SD (‰) | $\Delta^{201}$Hg (‰) | 2SD (‰) |
|---|---|---|---|---|---|---|---|---|---|---|
| Metamorphic basement rocks | | | | | | | | | | |
| PT11-1 | Two-mica quartz schist (Jitang Group) | 0.05 | | | −0.98 | 0.00 | −0.08 | 0.02 | −0.10 | 0.02 |
| JT11-2 | Feldspar two-mica quartz schist (Jitang Group) | 0.15 | | | 0.62 | 0.03 | −0.16 | 0.05 | −0.07 | 0.07 |
| Upper Triassic sedimentary rocks (barren rocks) | | | | | | | | | | |
| CN11-19 | Sandy slate (Adula Formation) | 0.04 | | | −1.77 | 0.11 | 0.00 | 0.06 | 0.00 | 0.03 |
| CN11-19 | Sandy slate[a] (Adula Formation) | 0.03 | | | −1.88 | 0.11 | −0.02 | 0.06 | −0.04 | 0.03 |
| LNM11-25 | Marlstone (Bolila Formation) | 0.08 | 19 | 55 | −1.33 | 0.21 | 0.06 | 0.01 | −0.01 | 0.07 |
| LNM11-27 | Argillaceous slate (Adula Formation) | 0.02 | 20 | 107 | −0.34 | 0.20 | −0.01 | 0.14 | −0.04 | 0.04 |
| LNM11-29 | Yellow feldspar greywacke (Duogaila Formation) | 0.04 | 18 | 30 | −0.86 | 0.11 | −0.03 | 0.06 | −0.08 | 0.00 |
| Upper Triassic sedimentary rocks (altered rocks) | | | | | | | | | | |
| LNM11-16 | Red feldspathic quartz sandstone (Jipila Formation) | 0.56 | 155 | 352 | −0.37 | 0.21 | −0.03 | 0.01 | 0.00 | 0.03 |
| LNM11-3 | Micritic limestone (Bolila Formation) | 1.89 | 1501 | 485 | −0.11 | 0.00 | 0.00 | 0.02 | −0.06 | 0.01 |
| vLNM-6 | Bioclastic limestone (Bolila Formation) | 2.34 | | | 0.53 | 0.28 | −0.17 | 0.03 | −0.01 | 0.02 |
| LNM11-24 | Micritic limestone (Bolila Formation) | 2.65 | 379 | 63 | −0.61 | 0.25 | 0.04 | 0.02 | 0.06 | 0.04 |
| CN11-12 | Quartz sandstone (Adula Formation) | 0.37 | 1750 | 10,000 | −0.31 | 0.08 | −0.16 | 0.04 | −0.21 | 0.04 |
| CN11-13 | Quartz sandstone (Adula Formation) | 0.24 | 308 | 8900 | 1.41 | 0.09 | −0.14 | 0.03 | −0.21 | 0.04 |
| Jurassic sedimentary rocks | | | | | | | | | | |
| JT11-20-1 | Lithic sandstone | 0.05 | 19 | 86 | −1.11 | 0.00 | −0.06 | 0.02 | 0.01 | 0.01 |
| JT11-21 | Quartz sandstone | 0.05 | | | −0.96 | 0.00 | −0.04 | 0.02 | −0.09 | 0.02 |
| JT11-22 | Lithic sandstone | 0.04 | | | −1.63 | 0.00 | 0.02 | 0.02 | −0.06 | 0.02 |

[a] Replicate sample; Pb and Zn concentrations are from Tao (2012)

Generally speaking, metamorphic basement and Jurassic rocks have low THg concentrations of 0.05 to 0.15 ppm, (with an average of 0.10 ppm) and 0.04 to 0.05 ppm (with an average of 0.05 ppm), respectively. Noticeably, THg concentrations greatly vary in Upper Triassic rocks (0.02 to 2.65 ppm, with an average of 0.75 ppm), some of which are probably associated with hydrothermal alteration. So we divided these Upper Triassic rocks into two groups. One group defined as altered rocks is collected from the geochemical halo of the hydrothermal system, and the other defined as barren rocks can represent regional background (Table 1).

THg concentrations of sulfides from Lanuoma and Cuona range from 62.9 to 1185 and 0.35 to 192 ppm, respectively (Table 2), significantly higher than those of the metamorphic basement and sedimentary rocks. The Lanuoma sphalerite displays high THg concentrations (436 to 1185 ppm), obviously higher than late-stage robinsonite (62.9 to 338 ppm). At Cuona, sphalerite (52.1 to 192 ppm) is also enriched in Hg, compared to intergrown galena (0.35 to 54.4 ppm). Our results lend support to the conclusion that Hg in Pb-Zn deposits is mainly hosted in sphalerite (Schwartz 1997; Grammatikopoulos et al. 2006).

## Hg isotope compositions

### *Metamorphic basement and sedimentary rocks*

An overall variation of 3.3‰ in $\delta^{202}$Hg values is observed for all rocks (Table 1). Metamorphic basement rocks and altered Upper Triassic rocks have mean $\delta^{202}$Hg values of −0.18 ± 1.13‰ ($n$ = 2, 1SD) and 0.09 ± 0.74‰ ($n$ = 6, 1SD), respectively. The barren Upper Triassic rocks and Jurassic rocks have mean $\delta^{202}$Hg values of −1.24 ± 0.64‰ ($n$ = 5, 1SD) and −1.23 ± 0.35‰ ($n$ = 3, 1SD), respectively, obviously lighter than the basement and altered Upper Triassic rocks. Our results are consistent with previous observations by Smith et al. (2008), who reported that $\delta^{202}$Hg values in sedimentary rocks (averaging −0.63 ± 0.24‰, $n$ = 16, 1SD) are lower than those in metamorphic rocks (averaging −0.31 ± 0.78‰, $n$ = 10, 1SD) from the California Coast Ranges (USA).

The variation in $\Delta^{199}$Hg values for all rocks (−0.17 to 0.06‰) is about four times higher than the analytical uncertainty for UM-Almadén (±0.06‰, 2SD) (Table 1). Metamorphic basement rocks ($\Delta^{199}$Hg of −0.19 to −0.08‰) and altered Upper Triassic rocks ($\Delta^{199}$Hg of −0.17 to 0.04‰) show small but significant Hg-MIF. In contrast, Hg-MIF is absent in barren Upper Triassic sedimentary rocks (i.e., the regional background) ($\Delta^{199}$Hg of −0.03 to 0.06‰) and Jurassic rocks ($\Delta^{199}$Hg of −0.06 to 0.02‰).

### *Sulfide ores*

The Hg isotopic composition of sulfides from the Lanuoma and Cuona deposits is summarized in Table 2. $\delta^{202}$Hg values of sulfides from Lanuoma and Cuona range from −0.57 to 1.01‰, with an average of 0.02 ± 0.47‰ ($n$ = 14, 1SD), and from −0.50 to 0.66‰, with an average of 0.15 ± 0.38‰ ($n$ = 17, 1SD), respectively. The mean $\delta^{202}$Hg values of sulfides in the two deposits are similar ($t$ test, $p$ = 0.411). However, $\delta^{202}$Hg values differ between different minerals (Fig. 6a). At Lanuoma, sphalerite ($\delta^{202}$Hg values ranging from −0.57 to −0.05‰) displays a mean $\delta^{202}$Hg value of −0.31 ± 0.20‰ ($n$ = 7, 1SD), slightly lower than that of late-stage robinsonite ($\delta^{202}$Hg of −0.17 to 1.01‰, averaging 0.36 ± 0.43‰, $n$ = 7, 1SD) ($t$ test, $p$ = 0.003). At Cuona, sphalerite ($\delta^{202}$Hg of −0.36 to 0.66‰) has a mean $\delta^{202}$Hg value of 0.33 ± 0.37‰ ($n$ = 9, 1SD), higher than galena (−0.50 to 0.48‰, averaging −0.05 ± 0.29‰, $n$ = 8, 1SD) ($t$ test, $p$ = 0.036). Sulfides show an overall mean $\delta^{202}$Hg of 0.09 ± 0.42‰ ($n$ = 31, 1SD), consistent with previously published sphalerite with $\delta^{202}$Hg of −0.47 ± 0.47‰ ($n$ = 102, 1SD) from China (Yin et al. 2016) and −0.65 ± 0.67‰ ($n$ = 4, 1SD) worldwide (Sonke et al. 2010).

$\Delta^{199}$Hg values of −0.23 to −0.05‰ (averaging −0.09 ± 0.05, $n$ = 14, 1SD) and −0.30 to 0.07‰ (averaging −0.12 ± 0.09, $n$ = 17, 1SD) are observed in sulfides from Lanuoma and Cuona, respectively. There is no statistical difference in $\Delta^{199}$Hg of the sulfides between the two deposits ($t$ test, $p$ = 0.251). In contrast to $\delta^{202}$Hg values, $\Delta^{199}$Hg values between different minerals are similar. At Lanuoma, $\Delta^{199}$Hg values of sphalerite (−0.12 to −0.04‰, averaging −0.07 ± 0.03‰, $n$ = 7, 1SD) are similar to late-stage robinsonite (−0.23 to −0.05‰, averaging −0.10 ± 0.06, $n$ = 7, 1SD) ($t$ test, $p$ = 0.202). Similarly, $\Delta^{199}$Hg values of sphalerite and galena from the Cuona deposit range from −0.30 to 0.07‰ (averaging −0.14 ± 0.12‰, $n$ = 9, 1SD) and −0.16 to −0.02‰ (averaging −0.09 ± 0.05‰, $n$ = 8, 1SD), respectively, which also display no statistical difference ($t$ test, $p$ = 0.213). Noticeably, $\Delta^{199}$Hg of sulfides from both deposits are similar to the metamorphic basement and altered Upper Triassic rocks, i.e., the geochemical halo, but significantly different from other barren background sedimentary rocks (Fig. 6b).

# Discussion

## Mercury distribution in sulfides, metamorphic basement, and sedimentary rocks

The THg concentrations of the two metamorphic basement samples in this study (0.05 to 0.15 ppm) are higher than the average Hg level for metamorphic rocks (0.01 ppm) in China (Chi 2004). Altered Upper Triassic rocks, the host rocks of the Pb-Zn ores, also have extremely high Pb and Zn concentrations, ranging from 155 to 1750 and 63 to 10,000 ppm, respectively (Table 1). In addition, the altered country rocks

**Table 2** Hg concentrations and Hg isotopic compositions in sulfide minerals from the Lanuoma and Cuona deposits, Changdu area

| Sample no. | Mineral | THg (ppm) | $\delta^{202}$Hg (‰) | 2SD (‰) | $\Delta^{199}$Hg (‰) | 2SD (‰) | $\Delta^{201}$Hg (‰) | 2SD (‰) |
|---|---|---|---|---|---|---|---|---|
| Cuona deposit | | | | | | | | |
| CN-110 | Gn | 0.52 | 0.09 | 0.00 | −0.05 | 0.02 | −0.07 | 0.02 |
| CN-112 | Gn | 0.54 | 0.48 | 0.00 | −0.15 | 0.02 | −0.11 | 0.02 |
| CN-113 | Gn | 0.35 | −0.20 | 0.09 | −0.07 | 0.02 | −0.08 | 0.00 |
| CN-119 | Gn | 10.45 | −0.23 | 0.21 | −0.09 | 0.02 | −0.06 | 0.01 |
| CN-120 | Gn | 0.51 | −0.07 | 0.19 | −0.06 | 0.01 | −0.03 | 0.02 |
| CN-120 | Gn[a] | 0.51 | −0.07 | 0.00 | −0.02 | 0.02 | −0.09 | 0.02 |
| CN-125 | Gn | 54.45 | 0.09 | 0.08 | −0.16 | 0.01 | −0.13 | 0.03 |
| CN-126 | Gn | 37.15 | −0.50 | 0.00 | −0.09 | 0.02 | −0.11 | 0.02 |
| CN-110 | Sp | 134.95 | −0.21 | 0.11 | 0.00 | 0.06 | −0.04 | 0.03 |
| CN-112 | Sp | 52.05 | 0.61 | 0.20 | −0.30 | 0.14 | −0.20 | 0.04 |
| CN-112 | Sp[a] | 52.05 | 0.70 | 0.09 | −0.24 | 0.03 | −0.19 | 0.00 |
| CN-113 | Sp | 82.04 | 0.29 | 0.08 | −0.14 | 0.01 | −0.12 | 0.07 |
| CN-113 | Sp[a] | 82.04 | 0.36 | 0.03 | −0.10 | 0.05 | −0.17 | 0.03 |
| CN-116 | Sp | 54.63 | 0.61 | 0.09 | −0.21 | 0.03 | −0.23 | 0.00 |
| CN-119 | Sp | 56.98 | 0.36 | 0.03 | −0.20 | 0.05 | −0.16 | 0.07 |
| CN-120 | Sp | 191.92 | −0.36 | 0.21 | 0.07 | 0.02 | 0.00 | 0.01 |
| CN-126 | Sp | 68.84 | 0.58 | 0.08 | −0.18 | 0.01 | −0.17 | 0.03 |
| Lanuoma deposit | | | | | | | | |
| LNM-2 | Rbn | 62.91 | 1.01 | 0.09 | −0.23 | 0.03 | −0.13 | 0.00 |
| LNM-16 | Rbn | 74.00 | 0.82 | 0.06 | −0.10 | 0.08 | −0.04 | 0.05 |
| LNM-117 | Rbn | 337.61 | −0.17 | 0.08 | −0.09 | 0.01 | −0.06 | 0.03 |
| LNM-118 | Rbn | 67.00 | 0.15 | 0.05 | −0.09 | 0.08 | −0.07 | 0.05 |
| LNM-123 | Rbn | 81.13 | 0.35 | 0.05 | −0.09 | 0.08 | −0.13 | 0.05 |
| LNM-124 | Rbn | 73.95 | 0.34 | 0.05 | −0.07 | 0.08 | 0.01 | 0.05 |
| LNM-125 | Rbn | 72.12 | 0.00 | 0.05 | −0.05 | 0.08 | −0.03 | 0.05 |
| LNM-12 | Sp | 717.88 | −0.05 | 0.10 | −0.04 | 0.01 | −0.10 | 0.03 |
| LNM-13 | Sp | 501.48 | −0.57 | 0.08 | −0.07 | 0.01 | −0.09 | 0.03 |
| LNM-104 | Sp | 815.94 | −0.50 | 0.08 | −0.04 | 0.01 | −0.08 | 0.03 |
| LNM-118 | Sp | 715.03 | −0.16 | 0.08 | −0.12 | 0.01 | −0.07 | 0.03 |
| LNM-123 | Sp | 435.52 | −0.43 | 0.08 | −0.08 | 0.01 | −0.02 | 0.05 |
| LNM-124 | Sp | 1184.78 | −0.31 | 0.08 | −0.07 | 0.01 | −0.10 | 0.03 |
| LNM-125 | Sp | 558.46 | −0.18 | 0.08 | −0.07 | 0.01 | −0.14 | 0.03 |

*Gn* galena, *Sp* sphalerite, *Rbn* robinsonite

[a] Replicate sample

exhibit mean $\delta^{202}$Hg and $\Delta^{199}$Hg values similar to the sulfides (Fig. 6a, b), indicating that they were likely affected by the same hydrothermal fluids. In contrast, the barren Upper Triassic rocks exhibit low Pb and Zn concentrations, usually less than 20 and 110 ppm, respectively.

The enrichment of Hg in sulfides from both deposits is in agreement with previous observations of Hg-bearing sulfide minerals around the world (Schwartz 1997; Grammatikopoulos et al. 2006; Radosavljević et al. 2012). Hg is normally presented as substitution of $Zn^{2+}$, $Pb^{2+}$, $Sb^{2+}$, and $Fe^{2+}$ by $Hg^{2+}$ (Schwartz 1997; Rytuba 2003). Sphalerite is the chief host for mercury in Pb-Zn deposits, which exhibits a perfect substitution of Hg into Zn (Schwartz 1997; Grammatikopoulos et al. 2006).

## Mass-dependent fractionation

Hg-MDF can be caused by numerous processes like redox reactions, leaching, boiling, and mineral precipitation, all of which are common in hydrothermal systems (Smith et al. 2005, 2008; Sherman et al. 2009; Smith 2010). However, leaching of Hg from source rocks at high temperature does not bring about significant Hg-MDF (<±0.5‰) (Smith et al. 2008), and magmatic processes (e.g., partial melting, magma

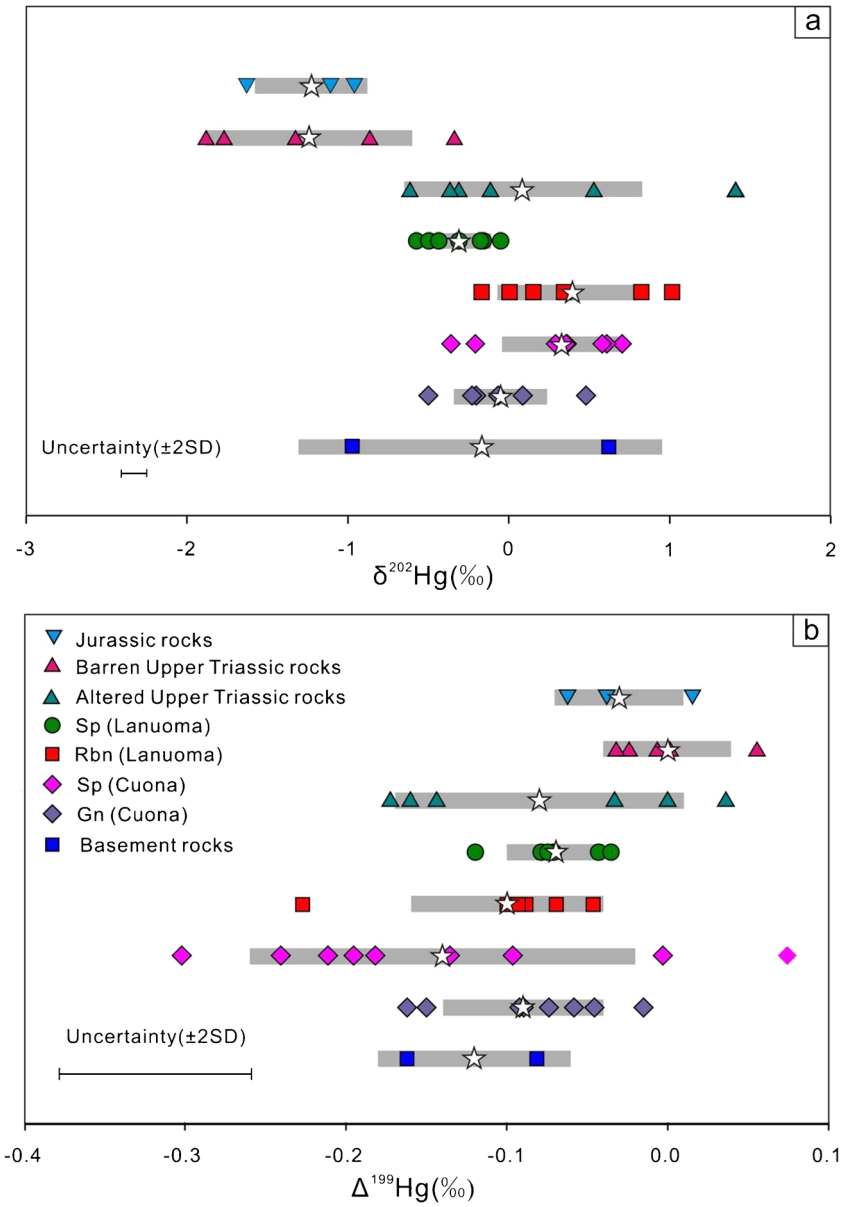


**Fig. 6** Variations in $\delta^{202}$Hg (**a**) and $\Delta^{199}$Hg (**b**) for sulfide minerals and potential source rocks from the Changdu area. *Star* symbol represents mean values of $\delta^{202}$Hg and $\Delta^{199}$Hg. *Gray shadow bar* represents 1SD uncertainty for mean values of $\delta^{202}$Hg and $\Delta^{199}$Hg

cooling, etc.) also cause limited isotope fractionation of Hg (Sherman et al. 2009). Recent researches reveal that large Hg-MDF (5‰ in $\delta^{202}$Hg) is likely to be caused by boiling of hydrothermal fluids associated with Hg(0) vaporization (Smith et al. 2005, 2008). This is further confirmed by laboratory experiments that Hg(0) vaporization can cause Hg-MDF of ≥1‰ in $\delta^{202}$Hg with Hg(0) preferentially enriched with isotopically lighter Hg (Zheng et al. 2007). Our results show variations of ~1.6 and ~1.2‰ in $\delta^{202}$Hg in sulfides from the Lanuoma and Cuona deposits, respectively. Such kind of large variations of $\delta^{202}$Hg (~3‰) was also reported in sphalerite from different types of Pb-Zn deposits worldwide (Sonke et al. 2010; Yin et al. 2016). However, the ranges of $\delta^{202}$Hg in sulfides from this study are much smaller than those reported for Hg ore deposits from northern Nevada and the California Coast Ranges ($\delta^{202}$Hg ~5‰), which are affected by boiling of ore-forming fluids (Smith et al. 2005, 2008), but they are similar to those reported for sphalerite from the Mississippi Valley-type deposits ($\delta^{202}$Hg ~1.2 ‰), the latter was formed without boiling (Smith 2010). According to the fluid inclusion data, there is a lack of evidence for boiling during sulfide formation at Lanuoma (Tao et al. 2011). Previous study has revealed that the presence of aqueous inclusions with variable vapor/liquid proportions in the same sample can indicate boiling (Sherlock et al. 1995). However, only aqueous fluid inclusions are observed at Lanuoma, and they typically exhibit ~20% vapor phase by volume and are homogenized to liquid upon heating (Tao et al. 2011). Fluid inclusion data for the

Cuona deposit is unavailable, because there is lack of appropriate minerals for microthermometric measurements. Overall, we think the variations of $\delta^{202}$Hg in sulfides from both deposits are not caused by boiling.

As mentioned above, diagnostic changes in $\delta^{202}$Hg between different minerals are observed. The $\delta^{202}$Hg data of the early-stage sphalerite from Lanuoma are slightly lower than that of the coexisting robinsonite. We hypothesize that this is caused by kinetic fractionation of Hg during sulfide precipitation. Nearly all kinetic reactions can produce Hg products with lower $\delta^{202}$Hg and leave the residual pool of reactant with higher $\delta^{202}$Hg (Blum et al. 2014). The observation of slightly lighter $\delta^{202}$Hg values in sphalerite from Lanuoma suggests that sulfide precipitation is probably associated with small Hg-MDF. Isotope fractionation of Hg during Pb-Zn mineralization is still under investigation, and further studies are needed.

## Mass-independent fractionation

Two possible mechanisms can explain MIF of odd Hg isotopes (MIF), namely the nuclear volume effect (NVE) (Schauble 2007) and the magnetic isotope effect (MIE) (Buchachenko 2001). NVE can take place during processes like elemental Hg(0) evaporation (Estrade et al. 2009; Ghosh et al. 2013) and dark Hg(II) reduction (Zheng and Hintelmann 2010), generating MIF with a $\Delta^{199}$Hg/$\Delta^{201}$Hg ratio of ~1.6. MIE mainly occurs during photochemical reaction of Hg. Photochemical reaction may be the most responsible for the observed MIF in this study, because it generates large MIF that is almost one order of magnitude higher than in other processes (Bergquist and Blum 2009; Sonke 2011). Specifically, aqueous Hg(II) photoreduction processes are associated with $\Delta^{199}$Hg/$\Delta^{201}$Hg ratios of 1.0 to 1.2 (Bergquist and Blum 2007; Zheng and Hintelmann 2009), whereas MeHg photodegradation results in a $\Delta^{199}$Hg/$\Delta^{201}$Hg ratio of 1.36 (Bergquist and Blum 2007). All rocks and sulfides in our study have a $\Delta^{199}$Hg/$\Delta^{201}$Hg ratio of 1.29 ± 0.29 (2SE) (Fig. 7), which was more likely to be caused by Hg(II) photoreduction, because MeHg is usually lower than Hg(II) in environmental and geological samples by more than an order of magnitude (Blum et al. 2014; Yin et al. 2016).

Hg-MIF have been shown in shale and sphalerite, and the MIF were mainly explained by mobilization of sedimentary Hg with significant MIF (Blum and Anbar 2010; Sonke et al. 2010; Yin et al. 2016). Leaching of Hg from sedimentary rocks and subsequent hydrothermal transportation seem unlikely to alter the MIF signature of Hg in sphalerite (Sonke et al. 2010; Yin et al. 2016). Hence, we consider significant Hg-MIF (~0.4‰ in $\Delta^{199}$Hg) in the Lanuoma and Cuona deposits could be used to trace the metal sources. These two investigated deposits are catalogued as sediment-hosted Pb-Zn deposits, which have no obvious genetic association with igneous activity (He et al. 2009; Song et al. 2011). Ore-forming fluids responsible for these deposits are formed from basinal brines with their metals derived from a variety of crustal sources (Leach et al. 2005). Hg-MIF has been reported for numerous sediment-hosted Pb-Zn deposits such as MVT ($\Delta^{199}$Hg ~0.4‰) and SEDEX ($\Delta^{199}$Hg ~0.3‰) deposits from China (Yin et al. 2016) and carbonate-hosted Zn-Cu deposit (~0.12‰ in $\Delta^{199}$Hg) from Congo (Sonke et al. 2010). In contrast, those Pb-Zn deposits related with igneous intrusions generally exhibit insignificant Hg-MIF (Yin et al. 2016). Previous studies also revealed Hg-MIF signatures are absent in igneous rocks and mantle-derived magmas (Smith et al. 2008; Sherman et al. 2009). We suggest that MIF in

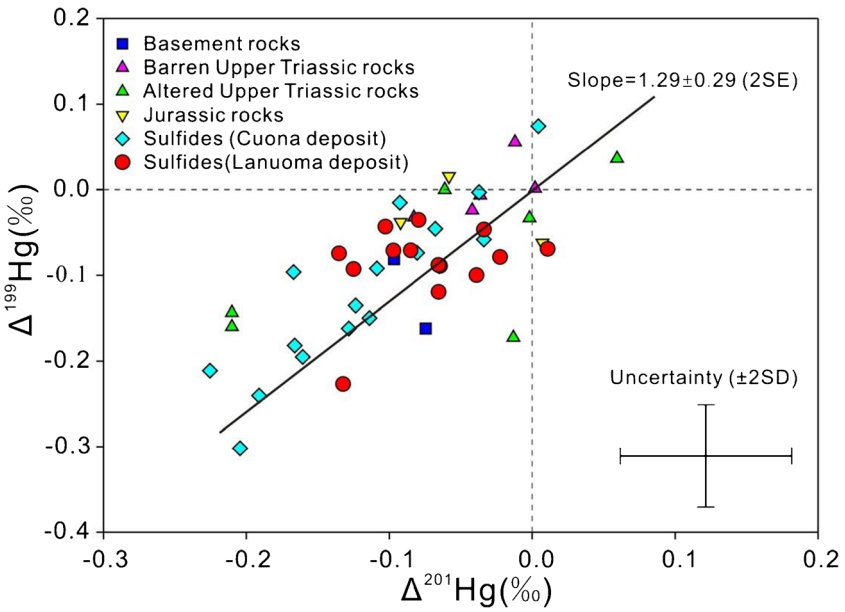


**Fig. 7** Plot of $\Delta^{199}$Hg versus $\Delta^{201}$Hg for sulfide minerals and potential source rocks from the Changdu area. The regression line is calculated by the York regression method (York 1968), which takes into account uncertainties in both $\Delta^{201}$Hg and $\Delta^{199}$Hg (slope = 1.29 ± 0.29, 2SE)

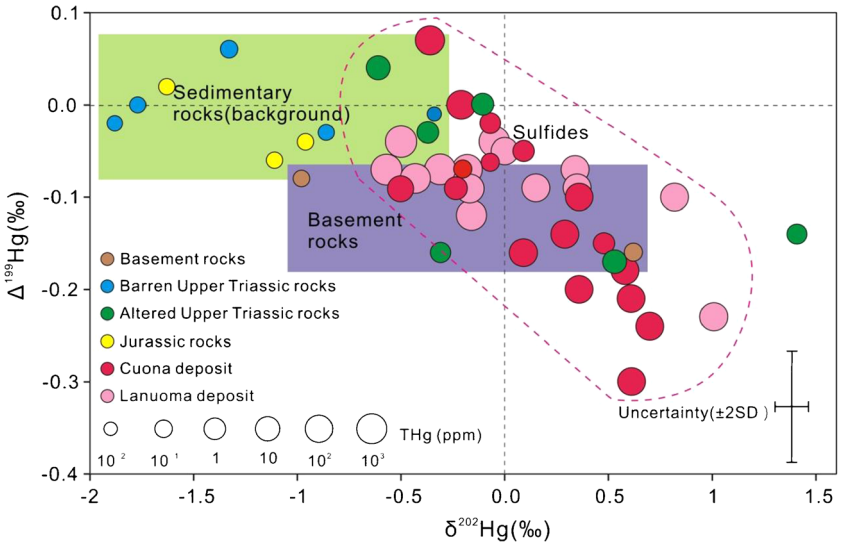


**Fig. 8** Plot of $\Delta^{199}$Hg versus $\delta^{202}$Hg for sulfide minerals and potential source rocks from the Changdu area

sulfides from the Lanuoma and Cuona deposits may be inherited from metamorphic basement rocks, since Hg-MIF is only observed in them. These metamorphic basement rocks were collected from regional area far away from the Pb-Zn deposits (Fig. 1b), which can rule out the possibility of hydrothermal alteration. Basement rocks might be an important Hg source for the Lanuoma and Cuona deposit. Previous studies also confirmed that basement rocks could be an important source of metals for Pb-Zn deposits (Goldhaber et al. 1995; Wilkinson et al. 2005; Moroskat et al. 2015). Lead isotopes for several sediment-hosted Pb-Zn deposits, including Irish Midlands, Southeast Missouri, and Tri-State, are indicative of a significant component from basement-derived Pb (Goldhaber et al. 1995; Wilkinson et al. 2005).

We assume that whether Hg-MIF occurs in different rocks depends on rock types. The protolith of the two-mica schist metamorphic rocks in this study is argillaceous, which is comprised of soils (Li et al. 2009). Negative MIF has been observed in soils (Zhang et al. 2013; Jiskra et al. 2015). Triassic and Jurassic sedimentary rocks are mainly limestone and sandstone, which were formed in shallow marine environment (Du et al. 1997). Shallow marine receives negative MIF from watershed soils (Zhang et al. 2013; Jiskra et al. 2015) and positive MIF from precipitation (Gratz et al. 2010; Chen et al. 2012). Mixing of soil Hg and precipitation Hg may result in less to no MIF in the Triassic and Jurassic sedimentary rocks.

### Implications for ore deposit formation

Figure 8 illustrates the systemic variations of Hg concentrations and Hg isotopic compositions in the Lanuoma and Cuona deposits. Due to the limited MDF and MIF of Hg isotopes during mineralization, the variations of Hg isotopes could be explained by mixing of Hg derived from several isotopically distinct sources. During the Cenozoic Indo-Asian collision, orogenic fluids migrated along gently-dipping detachment faults of the thrust systems towards the basin and leached Hg and other metals from deep-seated basement rocks (Hou et al. 2008). When the ore-forming fluids (with negative $\Delta^{199}$Hg and higher $\delta^{202}$Hg) ascended along the faults, they mixed with Hg from country rocks (with $\Delta^{199}$Hg of 0 and lower $\delta^{202}$Hg). Some sulfides have $\delta^{202}$Hg and $\Delta^{199}$Hg values out of the range of the rock samples, which may be due to the limited number of rock samples studied.

## Conclusion

This study documents dramatic changes in MDF-MIF signatures of Hg isotopes in two individual sediment-hosted Pb-Zn deposits from the Changdu area, SW China. Variations of Hg isotopes in these two deposits are indicative of mixing of hydrothermal fluids from different sources. The MIF signature in the sulfides is likely to be inherited from basement rocks which also show significant MIF. This study sheds new light on Hg isotopes as a geochemical tracer for metal sources and provides insights that basement rocks may be an important source of Hg (and probably also Pb-Zn) for the investigated sediment-hosted Pb-Zn deposits.

**Acknowledgements** This research was supported by the National Key Basic Research Program of China (973 Program) (2015CB452603, 2009CB421005) and National Natural Science Foundation of China (41303014). We thank Dr. Zhonggen Li and Dr. Buyun Du for helping with THg concentration analysis. Also, Dr. Nengping Shen and Dr. Jiehua Yang are acknowledged for their aid with field sampling. We acknowledge the USGS Wisconsin Mercury Research Lab and Wisconsin State Lab of Hygiene for the use of their lab space and multicollector ICP-MS for the determination of stable Hg isotopes. Dr. Bernd Lehmann and several anonymous reviewers are thanked for their constructive comments that have largely improved the quality of this paper.

## References


Bergquist BA, Blum JD (2007) Mass-dependent and independent fractionation of Hg isotopes by photoreduction in aquatic systems. Science 318:417–420

Bergquist BA, Blum JD (2009) The odds and evens of mercury isotopes, applications of mass-dependent and mass-independent isotope fractionation. Elements 5:353–357

Blum JD, Anbar AD (2010) Mercury isotopes in the late Archean Mount McRae Shale. Geochim Cosmochim Acta 74:A98–A98

Blum JD, Bergquist BA (2007) Reporting of variations in the natural isotopic composition of mercury. Anal Bioanal Chem 388:353–359

Blum JD, Sherman LS, Johnson MW (2014) Mercury isotopes in earth and environmental sciences. Annu Rev Earth Planet Sci 42:249–269

Bouhlel S, Leach DL, Johnson CA, Marsh E, Salmi-Laouar S, Banks DA (2016) A salt diapir-related Mississippi Valley-type deposit: the Bou Jaber Pb-Zn-Ba-F deposit, Tunisia: fluid inclusion and isotope study. Mineral Deposita 51:1–32

Buchachenko AL (2001) Magnetic isotope effect: nuclear spin control of chemical reactions. J Phys Chem A 105:9995–10011

Chen J, Hintelmann H, Feng X, Dimock B (2012) Unusual fractionation of both odd and even mercury isotopes in precipitation from Peterborough, ON, Canada. Geochim Cosmochim Acta 90:33–46

Chi Q (2004) Abundance of mercury in crust, rocks and loose sediment. Geochimica 33:641–648 (in Chinese with English abstract)

Das R, Salters VJ, Odom AL (2009) A case for in vivo mass-independent fractionation of mercury isotopes in fish. Geochem Geophy Geosy 10:1–12

Deloule E, Allegre CJ, Doe BR (1986) Lead and sulfur isotope microstratigraphy in galena crystals from Mississippi Valley-type deposits. Econ Geol 81:1307–1321

Du D, Luo J, Li X (1997) Sedimentary evolution and palaeogeography of the Qamdo Block in Xizang. Sediment Facies Palaeogeogr 17:1–17 (in Chinese with English abstract)

Estrade N, Carignan J, Sonke JE, Donard OFX (2009) Mercury isotope fractionation during liquid–vapor evaporation experiments. Geochim Cosmochim Acta 73:2693–2711

Estrade N, Carignan J, Donard OF (2010) Isotope tracing of atmospheric mercury sources in an urban area of northeastern France. Environ Sci Technol 44:6062–6067

Feng D (2006) Evaluation report on Lanuoma lead-zinc polymetallic deposit, Changdu basin, Tibet. Institute of Geological Survey of Tibet Autonomous Region (in Chinese)

Feng X, Foucher D, Hintelmann H, Yan H, He T, Qiu G (2010) Tracing mercury contamination sources in sediments using mercury isotope compositions. Environ Sci Technol 44:3363–3368

Foucher D, Ogrinc N, Hintelmann H (2009) Tracing mercury contamination from the Idrija mining region (Slovenia) to the Gulf of Trieste using Hg isotope ratio measurements. Environ Sci Technol 43:33–39

Gantner N, Hintelmann H, Zheng W, Muir DC (2009) Variations in stable isotope fractionation of Hg in food webs of Arctic lakes. Environ Sci Technol 43:9148–9154

Ghosh S, Schauble EA, Couloume GL, Blum JD, Bergquist BA (2013) Estimation of nuclear volume dependent fractionation of mercury isotopes in equilibrium liquid–vapor evaporation experiments. Chem Geol 336:5–12

Goldhaber MB, Church SE, Doe BR, Aleinikoff JN, Brannon JC, Podosek FA, Mosier EL, Taylor CD, Gent CA (1995) Lead and sulfur isotope investigation of Paleozoic sedimentary rocks from the southern midcontinent of the United States; implications for paleohydrology and ore genesis of the Southeast Missouri lead belts. Econ Geol 90:1875–1910

Grammatikopoulos TA, Valeyev O, Roth T (2006) Compositional variation in Hg-bearing sphalerite from the polymetallic Eskay Creek deposit. British Columbia, Canada Chem Erde-Geochem 66:307–314

Gratz LE, Keeler GJ, Blum JD, Sherman LS (2010) Isotopic composition and fractionation of mercury in Great Lakes precipitation and ambient air. Environ Sci Technol 44:7764–7770

He L, Song Y, Chen K, Hou Z, Yu F, Yang Z, Wei J (2009) Thrust-controlled, sediment-hosted, Himalayan Zn–Pb–Cu–Ag deposits in the Lanping foreland fold belt, eastern margin of Tibetan Plateau. Ore Geol Rev 36:106–132

Hintelmann H, Lu S (2003) High precision isotope ratio measurements of mercury isotopes in cinnabar ores using multi-collector inductively coupled plasma mass spectrometry. Analyst 128:635–639

Hintelmann H, Zheng W (2012) Tracking geochemical transformations and transport of mercury through isotope fractionation. In: Liu G, Cai Y, O'driscoll N (eds) Environmental chemistry and toxicology of mercury. Wiley, New York, pp 293–327

Hou Z, Cook NJ (2009) Metallogenesis of the Tibetan collisional orogen: a review and introduction to the special issue. Ore Geol Rev 36:2–24

Hou Z, Zaw K, Pan G, Mo X, Xu Q, Hu Y, Li X (2007) Sanjiang Tethyan metallogenesis in SW China: tectonic setting, metallogenic epochs and deposit types. Ore Geol Rev 31:48–87

Hou Z, Song Y, Zheng L, Wang Z, Yang Z, Yang Z (2008) Thrust-controlled, sediments-hosted Pb-Zn-Ag-Cu deposits in eastern and northern margins of Tibetan orogenic belt, geological features and tectonic model. Miner Depos 27:123–144 (in Chinese with English abstract)

Jiskra M, Wiederhold JG, Skyllberg U, Kronberg RM, Hajdas I, Kretzschmar R (2015) Mercury deposition and re-emission pathways in boreal forest soils investigated with Hg isotope signatures. Environ Sci Technol 49:7188–7196

Kesler SE, Cumming GL, Krstic D, Appold MS (1994) Lead isotope geochemistry of Mississippi Valley-type deposits of the southern Appalachians. Econ Geol 89:307–321

Krahn L, Baumann A (1996) Lead isotope systematics of epigenetic lead-zinc mineralization in the western part of the Rheinisches Schiefergebirge, Germany. Mineral Deposita 31:225–237

Leach DL, Sangste DF, Kelley KD, Large RR, Garven G, Allen CR, Gutzmer J, Walters S (2005) Sediment-hosted lead-zinc deposits, a global perspective. Econ Geol 100:561–607

Leach DL, Bradley DC, Huston D, Pisarevsky SA, Taylor RD, Gardoll SJ (2010) Sediment-hosted lead-zinc deposits in Earth history. Econ Geol 105:593–625

Li Z, Feng X, He T (2005) Determination of total mercury in soil and sediment by aquaregia digestion in the water bath coupled with cold vapor atom fluorescence spectrometry. Bull China Soc Miner Petrol Geochem 24:140–143 (in Chinese with English abstract)

Li C, Xie Y, Dong Y, Jiang G (2009) Discussion on the age of Jitang Group around Leiwuqi area, eastern Tibet, China and primary understanding. Geol Bull China 28:1178–1180 (in Chinese with English abstract)

Moroskat M, Gleeson SA, Sharp RJ, Simonetti A, Gallagher CJ (2015) The geology of the carbonate-hosted Blende Ag–Pb–Zn deposit, Wernecke Mountains, Yukon, Canada. Mineral Deposita 50:83–104

Peng Y, Wang M, Chen M (2000) The Qamdo-Riwoqe Triassic cratonic basin in eastern Xizang, sequence stratigraphy and correlation. Sediment Geol Tethyan Geol 20:62–67 (in Chinese with English abstract)

Pribil MJ, Gray J, Van Metre P, Borrok D, Thapalia A (2010) Tracing anthropogenic contamination in a lake sediment core using Hg, Pb, and Zn isotopic compositions. 2010 GSA Denver Annual Meeting

Radosavljević SA, Stojanović JN, Pačevski AM (2012) Hg-bearing sphalerite from the Rujevac polymetallic ore deposit, Podrinje Metallogenic District, Serbia: compositional variations and zoning. Chem Erde-Geochem 72:237–244

Rytuba JJ (2003) Mercury from mineral deposits and potential environmental impact. Environ Geol 43:326–338

Schauble EA (2007) Role of nuclear volume in driving equilibrium stable isotope fractionation of mercury, thallium, and other very heavy elements. Geochim Cosmochim Acta 71:2170–2189

Schwartz MO (1997) Mercury in zinc deposits: economic geology of a polluting element. Int Geol Rev 39:905–992

Sherlock RL, Tosdal RM, Lehrman NJ, Graney JR, Losh S, Jowett EC, Kesler SE (1995) Origin of the McLaughlin Mine sheeted vein complex; metal zoning, fluid inclusion, and isotopic evidence. Econ Geol 90:2156–2181

Sherman LS, Blum JD, Nordstrom DK, McCleskey RB, Barkay T, Vetriani C (2009) Mercury isotopic composition of hydrothermal systems in the Yellowstone Plateau volcanic field and Guaymas Basin sea-floor rift. Earth Planet Sci Lett 279:86–96

Singer DA (1995) World class base and precious metal deposits—a quantitative analysis. Econ Geol 90:88–104

Smith CN (2010) Isotope geochemistry of mercury in active and fossil hydrothermal systems. Dissertation, University of Michigan

Smith CN, Kesler SE, Klaue B, Blum JD (2005) Mercury isotope fractionation in fossil hydrothermal systems. Geology 33:825–828

Smith CN, Kesler SE, Blum JD, Rytuba JJ (2008) Isotope geochemistry of mercury in source rocks, mineral deposits and spring deposits of the California Coast Ranges, USA. Earth Planet Sci Lett 269:399–407

Song Y, Hou Z, Yang T, Zhang H, Yang Z, Tian S, Liu Y, Wang X, Liu Y, Xue C (2011) Sediment-hosted Himalayan base metal deposits in Sanjiang region, characteristics and genetic types. Acta Petrol Mineral 30:355–380 (in Chinese with English abstract)

Sonke JE (2011) A global model of mass independent mercury stable isotope fractionation. Geochim Cosmochim Acta 75:4577–4590

Sonke JE, Schäfer J, Chmeleff J, Audry S, Blanc G, Dupré B (2010) Sedimentary mercury stable isotope records of atmospheric and riverine pollution from two major European heavy metal refineries. Chem Geol 279:90–100

Spurlin MS, Yin A, Horton BK, Zhou J, Wang J (2005) Structural evolution of the Yushu-Nangqian region and its relationship to syncollisional igneous activity, east-central Tibet. Geol Soc Am Bull 117:1293–1317

Tang J, Zhong K, Liu Z, Li Z, Dong S (2006) Intracontinent orogen and metallogenesis in Himalayan epoch, Changdu large composite basin, Eastern Tibet. Acta Geol Sin 80:1364–1376 (in Chinese with English abstract)

Tang Y, Bi X, Yin R, Feng X, Hu R (2017) Concentrations and isotopic variability of mercury in sulfide minerals from the Jinding Zn-Pb deposit, Southwest China. Ore Geol Rev. doi:10.1016/j.oregeorev.2016.12.009

Tao Y (2012) Ore forming processes of Zn-Pb-Cu-Ag deposits in the Changdu Basin: mechanisms of elemental paragenesis, separation and super enrichment. Annual Report of National Basic Research Program (2009CB421005), Guiyang (in Chinese)

Tao Y, Bi X, Xin Z, Zhu F, Liao M, Li Y (2011) Geology, geochemistry and origin of Lanuoma Pb–Zn–Sn deposit in Changdu area, Tibet. Miner Depos 30:599–615 (in Chinese with English abstract)

Wilkinson JJ, Eyre SL, Boyce AJ (2005) Ore-forming processes in Irish-type carbonate-hosted Zn-Pb deposits: evidence from mineralogy, chemistry, and isotopic composition of sulfides at the Lisheen mine. Econ Geol 100:63–86

Yin R, Feng X, Shi W (2010) Application of the stable-isotope system to the study of sources and fate of Hg in the environment, a review. Appl Geochem 25:1467–1477

Yin R, Feng X, Wang J, Li P, Liu J, Zhang Y, Chen J, Zheng L, Hu T (2013) Mercury speciation and mercury isotope fractionation during ore roasting process and their implication to source identification of downstream sediment in the Wanshan mercury mining area, SW China. Chem Geol 336:72–79

Yin R, Feng X, Chen J (2014) Mercury stable isotopic compositions in coals from major coal producing fields in China and their geochemical and environmental implications. Environ Sci Technol 48:5565–5574

Yin R, Feng X, Hurley JP, Krabbenhoft DP, Lepak RF, Hu R, Zhang Q, Li Z, Bi X (2016) Mercury isotopes as proxies to identify sources and environmental impacts of mercury in sphalerites. Sci Rep 6:18686. doi:10.1038/srep18686

York D (1968) Least squares fitting of a straight line with correlated errors. Earth Planet Sci Lett 5:320–324

Zhang H, Yin R, Feng X, Sommar J, Anderson CWN, Sapkota A, Fu X, Larssen T (2013) Atmospheric mercury inputs in montane soils increase with elevation: evidence from mercury isotope signatures. Sci Rep 3:3322. doi:10.1038/srep03322

Zheng W, Hintelmann H (2009) Mercury isotope fractionation during photoreduction in natural water is controlled by its Hg/DOC ratio. Geochim Cosmochim Acta 73:6704–6715

Zheng W, Hintelmann H (2010) Nuclear field shift effect in isotope fractionation of mercury during abiotic reduction in the absence of light. J Phys Chem A 114:4238–4245

Zheng W, Foucher D, Hintelmann H (2007) Mercury isotope fractionation during volatilization of Hg(0) from solution into the gas phase. J Anal Atom Spectrom 22:1097–1104